J Appl Electrochem (2012) 42:169–178
DOI 10.1007/s10800-012-0384-6

ORIGINAL PAPER

Stability of Pt–Co/C and Pt–Pd/C based oxygen reduction reaction electrocatalysts prepared at a low temperature by a combined impregnation and seeding process in PEM fuel cells

Chortip Termpornvithit · Nuchaporn Chewasatn · Mali Hunsom

Received: 10 November 2011 / Accepted: 20 January 2012 / Published online: 2 February 2012

Abstract The stability of Pt–Co/C and Pt–Pd/C electrocatalysts relative to that of a commercial Pt/C catalyst was measured in terms of the loss of the electrochemical surface area (ESA). The electrocatalytic activity was investigated in an acidic solution (0.3 M H_2SO_4) and in a single PEM fuel cell under H_2/O_2 conditions. In the acidic solution, the ESA of the catalyst decreased as the number of repeated potential cycles increased, which is likely to be due to dissolution of the different metals contained within the catalyst structure. In the fuel cell environment, the deterioration of the cell performance increased as the number of repeated potential cycles increased. Thus, the loss of cell performance may be related to the loss of the ESA. In addition, the loss of the catalyst's ESA affected the cell performance at low-, medium-, and high- current densities, indicating a loss of either the activation potential or an ohmic loss. Among the three electrocatalysts evaluated, the Pt–Co/C based one exhibited the highest electrocatalytic activity in both the acidic solution and in the fuel cell environment.

Keywords Stability · Pt-based electrocatalysts · Potential cycling · Impregnation and seeding

C. Termpornvithit · N. Chewasatn · M. Hunsom (✉)
Fuels Research Center, Department of Chemical Technology, Faculty of Science, Chulalongkorn University, 254 Phayathai Road, Bangkok 10330, Thailand
e-mail: mali.h@chula.ac.th

M. Hunsom
Center of Excellence on Petrochemical and Materials Technology (PETRO-MAT), Chulalongkorn University, 254 Phayathai Road, Bangkok 10330, Thailand

1 Introduction

The proton exchange membrane (PEM) fuel cell is held as one of the most promising candidates as a clean power source for electric vehicles or combustion engines in automotive transport. This is largely due to its high energy conservation efficiency, the possibility of using regenerative fuels, low or zero levels of emission of noxious or environmental pollutants, a low operating temperature requirement and a relatively quick start-up [1, 2]. However, the commercialization and utilization of PEM fuel cells in automotive applications is not currently widespread because of two major technical gaps; namely its high cost and a low reliability and durability [3].

In practice, highly dispersed platinum (Pt)-based nanoparticles supported on carbon (C) particles are used in fuel cells because, compared to other metals Pt possesses a high exchange current density for both the oxidation and reduction reactions in the fuel cell, a high resistance to chemical attack, excellent high-temperature characteristics and has stable electrical properties. However, Pt is an expensive metal and the world's supply of Pt is limited, resulting in a high investment cost for fuel cells. Indeed, the present cost of energy produced from PEM fuel cells is estimated at about $200 per kW [4], of which about 50% of the total cost is from the catalyst in the electrode [5, 6]. Thus, to promote the commercial viability of fuel cells, the development of a cost-effective, active, and stable electrocatalyst is required. Utilization of non-Pt catalysts, either as less precious metals, such as Ru, Pd, Au, and Ag [7–9], or as non-precious metal composite electrocatalysts, such as cobalt–polypyrrole–carbon (Co–PPY–C) [10], cyanamide-Fe–C [11], polyaniline-Fe/ethylene diamine-Co–C (PANI-Fe/EDA-Co–C) [11] and CoN_x/C [12], are one set of options to reduce the cost of the fuel cell. Another option

is to increase the proportion of Pt in the electrode that is actually utilized in the electrocatalytic process, such as by designing a bi-layer catalyst structure [13, 14], increasing the tortuosity and interfacial reaction surface area [15, 16] or designing the catalyst layer as a multi-layer configuration [17–19]. However, these approaches are still in the research stages and are currently far from being established let alone commercially viable. Indeed, the catalytic activity and stability currently obtained with these systems are too low in comparison with what is required for use as a practical electrocatalyst in fuel cells.

Another strategy to reduce the Pt requirement, and so lower the cost of the fuel cell, is to promote the catalytic activity, and particularly the activity of the oxygen reduction reaction (ORR), and to increase the stability of the electrocatalyst by the use of a Pt-based alloy electrocatalyst (Pt–M/C; where M is another metal). As mentioned by Bezerra et al. [3], the catalytic activity and the tolerance to chemical resistance depends not only on the nature of the Pt (*ex*. Pt–Pt distance, metal particle size and surface structure), but also on the second metal. The relationship between the activity-stability and the composition of Pt alloys and a pure Pt standard was defined as falling into four categories: (i) highly corrosive and highly active (M = Fe, Co, V or Mn) (ii) corrosive and highly active (M = Zn, Cu, Mo or Ni) (iii) stable, but less active (M = Zr, Cr or Ta) and (iv) stable and active (M = W or Ti) [20]. In actual applications for fuel cells; however, the activity as well as the stability of the Pt-based electrocatalyst is strongly dependent on not only the type of the second metal but also on the type of the precursor and support, the supporting strategy, and the heat-treatment strategy [21, 22].

Therefore, it is essential to optimize the catalyst synthesis procedure. Colón-Mercado et al. [23] compared the activity and stability of commercial Pt_xM_1 catalysts supported on Vulcan XC-72 carbon black (20% (w w^{-1}) metal loading; ETEK), and reported that the incorporation of Ni, Co, Fe or V as the second metal into the carbon-supported Pt enhanced the initial activity of the electrocatalyst compared to the Pt/C one. Both Pt/C and Pt–Co/C electrocatalysts showed similar behavior during the accelerated durability test and in fuel cell testing. Zignani et al. [24] evaluated the activity and stability of Pt–Co/C catalysts prepared at a low temperature using $NaBH_4$ as the reducing agent and $H_2PtCl_6{\cdot}6H_2O$ and $Co(OH)_2{\cdot}6H_2O$ as the precursors. They reported that the presence of Co in the electrocatalyst provided a higher ORR activity compared to that of the Pt/C. However, the magnitude of the reduction in the ORR activity during the repeated potential cycling of the as-prepared and the thermal treated Pt–Co/C electrocatalysts were both higher than that for the Pt/C. This is presumably due to the dissolution and re-deposition of Pt that then forms a surface layer of non-alloyed pure Pt. A series of three Pt_xNi/C (x = 1–3) NP catalysts, prepared using $NaBH_4$ as the reducing agent and $H_2PtCl_6{\cdot}6H_2O$ and $NiCl_2{\cdot}6H_2O$ as the metal precursors [25], revealed that the presence of Ni in the Pt catalyst, and thus partial replacement of Pt with Ni, clearly enhanced the catalytic reactivity of the Pt catalyst towards the ORR. This is likely to be due to the contraction of the Pt lattice causing changes in the electronic properties of Pt. In addition, the incorporation of Ni into Pt/C catalysts led to a greater resistance to sintering when compared to the Ni-free Pt/C electrocatalyst, and so a greater long-term stability of the Pt–Ni/C electrode [26].

Heat-treatment of Pt–Co/C electrocatalysts was found to induce the formation of a *d*-band vacancy in Pt particles, and so increased the catalytic activity [27]. However, some contradictory results relating to the effect of heat-treatment on the catalytic activity have been observed. For instance, heat-treatment of Pt alloy catalysts at 700 °C and higher not only improved the Pt electroactivity but also increased the catalyst particle size, resulting in a decreased active area as well as catalyst mass activity [28–30].

Based upon our previous reported results [31, 32], it is apparent that the preparation of Pt–Co/C and Pt–Pd/C electrocatalysts by the combined process of impregnation and seeding provided both a more uniform dispersion of the metal particles on the catalyst surface and a smaller size of the electrocatalyst compared with those produced without the seeding approach. In addition, it provided higher ORR kinetics in PEM fuel cells. In this study, the stability of Pt–Co/C and Pt–Pd/C electrocatalysts was explored by repeated potential cycling in both an acid electrolyte and in a fuel cell environment in comparison to that of a commercial Pt/C catalyst.

2 Experimental

2.1 Preparation of the Pt–Pd/C and Pt–Co/C electrocatalysts

The preparation of the Pt–Pd/C electrocatalyst was performed in the two elementary steps of seeding and impregnation. Initially, 3.5 ml of 20 g l^{-1} H_2PtCl_6 (Fluka) and 4.5 ml of 20 g l^{-1} $PdCl_2$ (99%, Kento) were mixed together. A 1% (w v^{-1}) carbon slurry was prepared by dispersing 0.1 g of the treated carbon black [22] in 10 ml of de-ionized water, sonicating at 80 °C for 1 h and then adjusting the solution to pH 1 with 1 M HCl. The seeding step was conducted by mixing approximately 10% (v v^{-1}) of the $H_2PtCl_6/PdCl_2$ solution with the carbon-black slurry and sonicating at 80 °C for 30 min. The electrocatalyst ions in aqueous solution were then reduced to Pt and Pd metal by the addition of 20 ml of 0.15 M $NaBH_4$ (98%, Alcan) and sonicating for 30 min at 80 °C, and then

harvested by vacuum-filtration of this suspension. The wet seeded powder was rinsed several times with de-ionized water to eliminate the excess reducing agent.

The impregnation step was performed by dispersing the obtained carbon powder covered by the seeded Pt–Pd metal in de-ionized water, sonicating for 30 min and then adding it to the remaining $H_2PtCl_6/PdCl_2$ solution (90%) at the appropriate amount to obtain the required electrocatalyst loading on the carbon support (40% (w w^{-1})). The mixture was reduced by the addition of 20 ml of 0.12 M $NaBH_4$ under sonication for 30 min to obtain the catalyst powder, which settled out of the solution/suspension. The electrocatalyst suspension was filtered, and the filtrate was washed thoroughly with de-ionized water and dried overnight at 110 °C.

For preparation of the Pt–Co/C electrocatalyst, a similar procedure to the above was carried out as above except using 2.795 ml of a 20 g l^{-1} $CoCl_2$ (98%, Fluka) solution in place of the $PdCl_2$ solution. The morphology of the obtained Pt–Pd/C and Pt–Co/C electrocatalysts, along with the commercial Pt/C one, were characterized using X-ray diffraction (XRD), on a Shimada LabX XRD-6000, and scanning electron microscopy with energy dispersive X-ray analysis (SEM-EDX) was performed on a JOEL JSM-5410LV scanning electron microscope.

2.2 Preparation of the diffusion layer, electrocatalyst ink and electrocatalyst-coated gas diffusion layer (GDL)

The diffusion layer was prepared by coating the carbon ink, prepared as previously reported [32], onto the gas diffusion layer (GDL) by brushing at a constant diffusion layer loading of around 2.0 mg cm^{-2}. The carbon ink-coated GDL was finally dried at 100 °C for 60 min at atmospheric pressure. The electrocatalyst ink was prepared by dispersing the Pt–Co/C (or commercial 40% (w w^{-1}) Pt/C (ETEK) or Pt–Pd/C) electrocatalyst in 2 ml of 1,2-dimethoxyethane (98% $C_4H_{10}O_2$, Fluka) and sonicating at room temperature for 30 min. The 5% (w v^{-1}) Nafion solution (Fluka) was then added to the mixture and sonicated at room temperature for 1 h. Next, the electrocatalyst ink was coated on the carbon ink-coated GDL by a spray gun (Crescendo, Model 175-7^{TM}) at room temperature using a liquid flow rate ranging from 0.15 to 0.3 ml min^{-1} with air as the driving gas, and then dried at 100 °C for 1 h. This procedure was repeated several times to obtain a catalyst loading on the GDL of 0.5 mg cm^{-2}.

2.3 Preparation of test specimens for stability tests

The stability of the as-prepared Pt–Pd/C and Pt–Co/C electrocatalysts, as well as the commercial Pt/C electrocatalyst, was tested in both an acid electrolyte and in a single PEM fuel cell. For the former environment, the electrocatalyst-coated GDL was cut as a 1 cm diameter circle. For the latter environment, the electrocatalyst-coated GDL was assembled in a single PEM fuel cell as follows. The 5% (w v^{-1}) Nafion solution was applied onto the catalyst surface of two electrocatalyst-coated GDLs by a brushing procedure, with the as-prepared electrocatalyst used for the cathode and the commercial Pt/C for the anode, and then aligned with the treated Nafion membranes (Electrochem, Inc.) as previously reported [33]. Compression was then performed using a compression mould (LP 20-Labtech) at 137 °C and 65 kg_f cm^{-2} for 150 s to form the membrane electrode assembly (MEA).

2.4 Stability test by potential cycling

The three-probe stability test of the electrocatalysts was conducted in an acid environment using the as-prepared electrocatalyst-coated GDLs as the working electrode, a Pt rod as the counter electrode and a Ag/AgCl reference electrode. The potential cycling was carried out using a Potentiostat/Galvanolstat (PG STATO 30, Autolab) in 200 ml of 0.3 M H_2SO_4 at a varying potential from −0.4 to +1.4 V at a scan rate of 20 mV s^{-1} with constant agitation at 500 rpm. The solution, at any given number of repeated potential cycles, was collected and the metal ion content was evaluated by inductively coupled plasma spectrophotometry (4300 DV, Perkin).

In the fuel cell environment, the obtained MEA with a constant active surface area of 5 cm^2 was mounted on commercial single-cell hardware (Electrochem, Inc.) and tested in a single-cell test station. Prior to testing the cell performance, the run-in stage was carried out under atmospheric pressure with a cell temperature of around 60 °C by feeding an equal flow rate of H_2 and O_2 (100 sccm each at 100% humidity). The current was drawn at a high density (>700 mA cm^{-2}) for a period of 6–12 h. Consequently, the performance of the single cell was evaluated in the form of current density–potential curves (polarization curves), monitored by a Potentiostat/Galvanostat at 60 °C and ambient pressure. During the evaluation, the polarization assay was carried out first, so as to obtain the polarization curve, and then switched to the potential cycling mode between −0.4 to +1.4 V at a scan rate of 50 mV s^{-1}. The potential cycle was then repeated until the required number of cycles was reached when it was then switched to the polarization mode. The consecutive cycles of polarization/potential cycling were repeated several times to get satisfactory data.

3 Results and discussion

3.1 Morphology of the Pt–Co/C and Pt–Pd/C electrocatalysts

Representative XRD patterns of the as-prepared Pt–Co/C and Pt–Pd/C electrocatalysts, along with the commercial Pt/C electrocatalyst for comparison, are shown in Fig. 1. The commercial Pt/C electrocatalyst revealed the characteristic diffraction pattern of face-centered cubic (fcc) Pt for [111], [200] and [220] at a 2θ of 39.82°, 46.22°, and 67.58°, respectively. In the presence of Co or Pd the Pt diffraction peaks were shifted to higher 2θ values (~40.8/40.9, 46.1/47.2, and 68.5/70.2 for Pt–Co/C/Pt–Pd/C and [111], [200] and [220], respectively) compared to that of the commercial Pt/C electrocatalyst. The lattice parameters of both the Pt–Co/C and Pt–Pd/C electrocatalysts (Table 1) were between those of pure fcc Pt (0.3923 nm), pure fcc Co (0.3545 nm), and Pd (0.3891 nm), indicating the contraction of the lattice, due to the particle substitution of Pt by Co or Pd in the fcc structure [34]. No characteristic peaks of metallic Co or Pd were detected in the XRD patterns of the Pt–Co/C and Pt–Pd/C electrocatalysts, respectively, but their presence cannot be discarded because, they may be present as very small nanoparticles or even in an amorphous form. The average particle size, calculated by Scherer's equation [35], ranged from 5.50 for the Pt/C down to 3.48 nm for the Pt–Pd/C with the Pt–Co/C being slightly larger but not that much different (Table 1). With respect to the Pt: M ratio (M = Co or Pd), a 1.66-fold higher Pt content was observed in the Pt–Co/C electrocatalyst than in the Pt–Pd/C electrocatalyst. To explain the effect of metal types on the Pt: M ratio, it is necessary to take into account the effect of the standard reduction potential (E^0) of the metal ions in the system. In the case of the Pt–Co/C electrocatalyst, due to the much higher standard reduction potential of the Pt ion ($E^0_{PtCl_4^{2-}} = 0.73$ V versus SHE) in comparison to that for the Co ion ($E^0_{Co^{2+}} = -0.28$ V versus SHE), the Pt ions are more easily reduced than the Co ions leading to a higher quantity of metallic Pt being deposited onto the carbon substrate [36]. However, the standard reduction potential of Pd ions ($E^0_{Pd^{2+}} = 0.83$ V versus SHE) is slightly greater than that of Pt ions, resulting in a faster reduction of Pd ions on the carbon substrate. The particle dispersion (N_S/N_T) of the different types of catalysts was also calculated from the equations developed by Van Del Klink [37], given below as Eqs. 1–3:

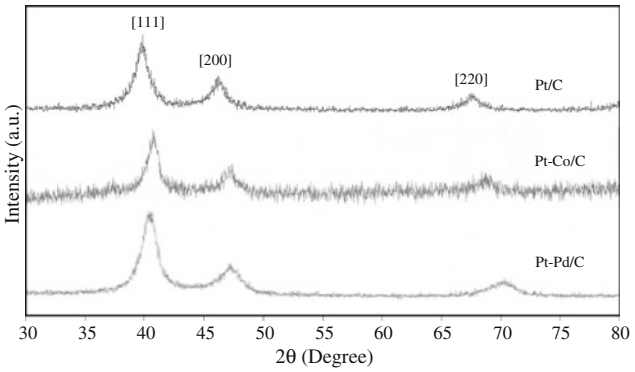

Fig. 1 Representative XRD patterns of the as-prepared Pt–Co/C and Pt–Pd/C electrocatalysts and the commercial Pt/C one. The *peaks* for the fcc Pt at [111], [200], and [220] are indicated

$$N_T = \frac{2\pi}{3}\left(\frac{d}{a}\right)^3 \quad (1)$$

$$N_T = \left(\frac{10}{3}\right)l^3 - 5l^2 + \left(\frac{11}{3}\right)l - 1 \quad (2)$$

$$N_S = 10l^2 - 20l + 12 \quad (3)$$

where N_T is the total number of atoms, N_S is the number of surface atoms, l is the number of layers, a is the lattice parameter and d is particle size of electrocatalyst.

The dispersion of both the Pt–Co/C and Pt–Pd/C electrocatalysts were nearly the same, being in the range of 33–34%, and were 1.44- to 1.49- fold higher than that of the commercial Pt/C catalyst (Table 1). The uniform particle dispersion of both the as-prepared Pt–Co/C and Pt–Pd/C electrocatalysts was also observed from the mapping (Fig. 2), confirming that a good particle dispersion of the electrocatalyst was obtained by this preparation procedure.

Figure 3 shows the current density-potential curve, or polarization curve, of a single PEM fuel cell in the presence of the three different types of electrocatalyst. It was clearly apparent that all three electrocatalysts exhibited an almost similar loss in current density at high cell potentials,

Table 1 Morphology of the as-prepared Pt–Co/C and Pt–Pd/C electrocatalysts compared with the commercial Pt/C

Electro-catalysts	Lattice parameters (nm)	Particle size (nm)	EDX (by atom)	Dispersion (N_S/N_T; %)	Initial ESA ($m^2\ g^{-1}$)	$MA_{0.75\ V}$ ($A\ mg^{-1}$)
Pt/C	0.3923	5.50	100:0	23.1	45.63	0.444
Pt–Co/C	0.3851	3.66	53:47	34.4	62.88	0.341
Pt–Pd/C	0.3914	3.48	32:68	33.3	109.2	0.310

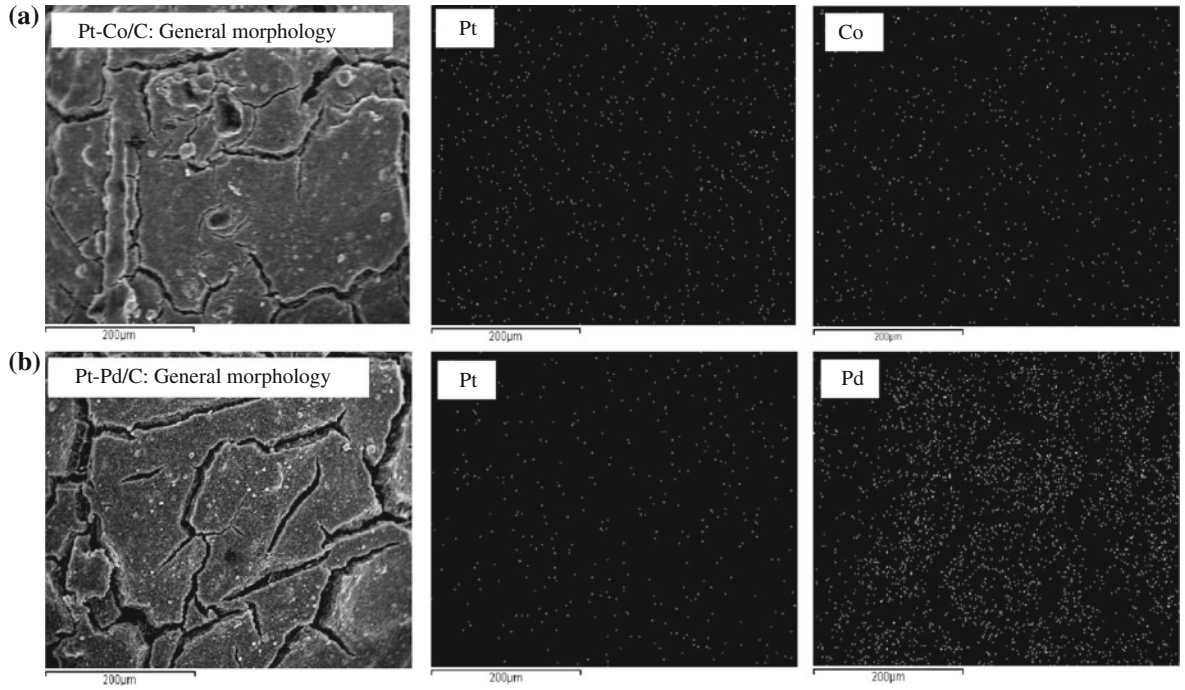

Fig. 2 SEM-EDX based element mapping of the as-prepared (**a**) Pt–Co/C and (**b**) Pt–Pd/C electrocatalysts by a combined impregnation and seeding process

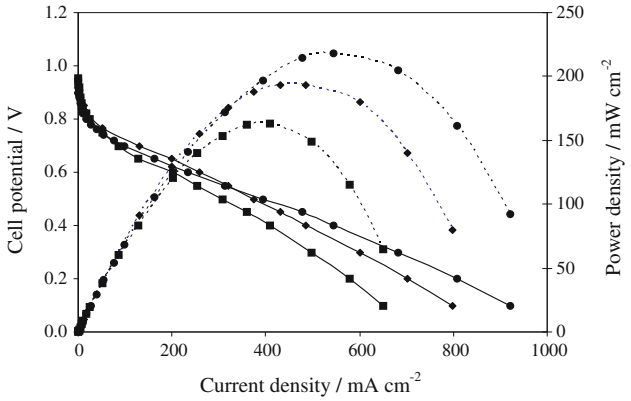

Fig. 3 Performance curve (*solid line*) and power density curve (*dotted line*) of the as-prepared Pt–Co/C (*filled square*) and Pt–Pd/C (*filled circle*) electrocatalysts and the commercial Pt/C (*filled diamond*)

or in other words an activation loss. The deviation of their performance was significantly observed at medium and high current densities. The mass activity ($MA_{0.75\ V}$), defined as the ratio between the current density in mA cm^{-2} at 0.75 V and the loading of metal in mg cm^{-2}, of the commercial Pt/C electrocatalyst was greater than those of the as-prepared Pt–Co/C and Pt–Pd/C electrocatalysts by around 1.30- and 1.43- fold, respectively, as shown in Table 1. However, for the whole cell potential range, the peak power of the cell with MEA in the presence of Pt–Pd/C (218 mW cm^{-2}) was noticeably higher than that measured in the cells with MEAs made with Pt/C and Pt–Co/C (194 and 164 mW cm^{-2}, respectively).

3.2 Electrocatalyst stability test in acid electrolyte

To test the electrocatalytic stability of each of the three different electrocatalyst types, an extremely corrosive condition was imitated by polarizing the electrocatalyst in acidic media (0.3 M H_2SO_4) between −0.4 to +1.4 V at a scan rate of 20 mV s^{-1} and with constant agitation at 500 rpm. The CV plots of the commercial Pt/C and the as-prepared Pt–Co/C and Pt–Pd/C electrocatalysts at room temperature during repeated potential cycles are shown in Fig. 4. For all three electrocatalysts, the adsorption potential of the hydrogen atom onto the Pt surface (Pt–H formation) was not observed as a sharp peak, in contrast to previous reports [38, 39]. Rather, it appeared as a broad shoulder and partially overlapped with the reduction peaks of the oxygen atom (Pt–O reduction). The degree of overlap increased as a function of the number of repeated potential cycles in all three electrocatalysts. In addition, the onset adsorption potential of the hydrogen atoms, as well as the reduction potential of the oxygen atoms, shifted to a negative value as the number of repeated potential cycles increased. This observed shift was only moderate for the Pt–Co/C and Pt–Pd/C electrocatalysts, but was much stronger for the commercial Pt/C electrocatalyst. This

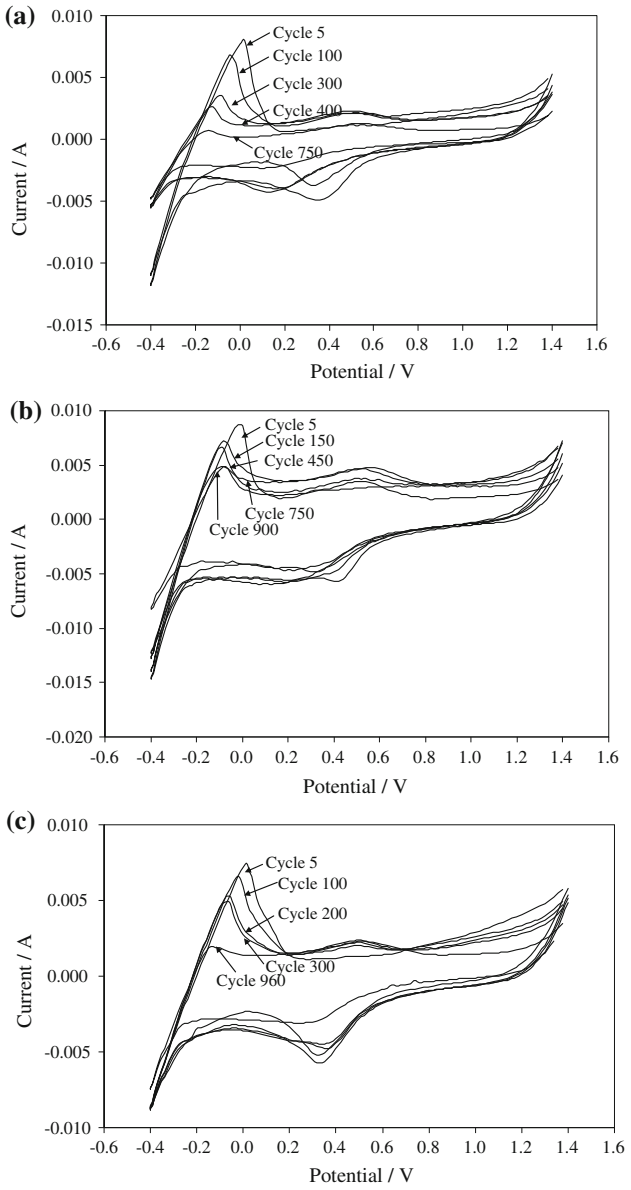

Fig. 4 CV curves of the (**a**) commercial Pt/C and the as-prepared (**b**) Pt–Co/C and (**c**) Pt–Pd/C electrocatalysts at a metal loading of 0.15 mg cm^{-2} after the indicated number of sequential potential cycles in 0.3 M H_2SO_4 at a scan rate of 20 mV s^{-1}

indicates the creation of a strongly adsorbed hydride as well as oxide layers on the Pt surface [40], resulting in the accumulation of an electronic charge on the electrocatalyst-electrolyte interface and also in the formation of a high double-layer charging current, particularly at higher numbers of repeated potential cycles.

With regard to the desorption potential of the hydrogen atom (Pt–H oxidation) for the electrocatalyst surface, strong wide peaks were observed with all three electrocatalysts. The onset desorption potential of hydrogen atoms shifted down field slightly as the number of repeat potential cycles increased. Also, the area under these curves decreased as the number of repeat potential cycles increased, indicating the variation in electrocatalyst surface area (ESA) [41].

The area under the peak of hydrogen desorption was used to calculate the ESA as in Eq. 4 [42]:

$$\mathrm{ESA} = \frac{Q_H}{[\mathrm{M}] \times 0.21} \tag{4}$$

where Q_H is the charge for hydrogen desorption, 0.21 is the charge required to oxidize a monolayer of H_2 on bright Pt and [M] is the metal loading of Pt on the electrode.

The initial ESA of the Pt–Co/C and Pt–Pd/C electrocatalysts were 62.88 and 109.2 m^2 g^{-1}, respectively, which were 1.38- and 2.39- fold higher than that of the commercial Pt/C catalyst, respectively (Table 1). Figure 5 shows the variation in the normalized ESA as a function of the number of repeated potential cycles, and clearly reveals that the ESA of all three electrocatalysts decreased as the number of potential cycles increased. The magnitude of the decreased ESA was great in the commercial Pt/C electrocatalyst, dropping to an almost 50 and 8.5% residual ESA level after 250 cycles and 600–750 cycles, respectively, and the least in the Pt–Co/C electrocatalyst where the ESA did not even drop to a 50% residual level but rather decreased to 68% residual ESA after 300 cycles and reached at a plateau at a minimum of 54.7% ESA from 650 cycles onwards. The decrease in the ESA of the Pt–Pd/C electrocatalyst was in between the other two, decreasing to 50% after 450 cycles and reached a minimum ESA level of 25.2% from 800 cycles onwards.

This decrease in the ESA could result from various mechanisms, such as Pt dissolution, re-deposition on the catalyst surface and Pt migration through the surface [23]. However, Pt dissolution into the electrolyte from the supported Pt catalysts is supported by the existence of

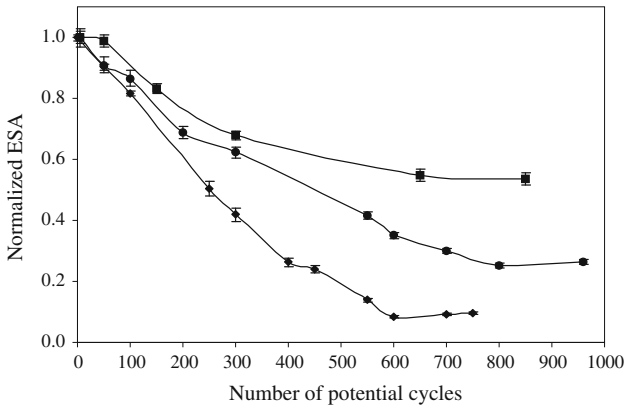

Fig. 5 The change in the ESA (normalized to the initial surface area) of the commercial Pt/C (*filled diamond*) and the as-prepared Pt–Co/C (*filled square*) and Pt–Pd/C (*filled circle*) electrocatalysts at a metal loading of 0.15 mg cm^{-2} after the indicated number of repeated potential cycles in 0.3 M H_2SO_4 at a scan rate of 20 mV s^{-1}

increasing levels of Pt ions in the electrolyte as the number of repeat potential cycles increased (Fig. 6a). These dissolved Pt ions can be re-deposited on the Pt surface, resulting in the formation of larger Pt nanoparticles, a phenomenon known as Ostwald ripening [43]. For the Pt–Pd/C electrocatalyst, a much smaller quantity of Pd ions were dissolved in the electrolyte than Pt ions, in accordance with the higher standard reduction potential for Pd than for Pt. For the Pt–Co/C electrocatalyst a greater than two-fold higher level of Co ions than Pt ions were found to be dissolved in the acid electrolyte, which is likewise attributed to the lower reduction standard potential of Co. According to these obtained results, the incorporation of the second metal (Co or Pd) into the Pt/C electrocatalyst structure improved the stability of the Pt/C electrocatalyst. This is likely to be because, the second metal helps to reduce the Pt mobility on the supporting material, and so results in a stronger bonding of the alloying metal atoms to the carbon powder, and in turn prevents sintering [40, 44]. This effect is sometimes called the "anchoring effect". As mentioned by Yu et al. [45] and Gasteiger et al. [46], the incorporation of Co onto the Pt catalyst can reduce Pt dissolution and migration during the course of operation and so result in an increased Pt–Co/C stability compared to that for the Pt/C electrocatalyst. In the case of the Pt–Pd/C electrocatalyst, Cho et al. [47] claimed that the presence of Pd particles helped to reconfigure the Pt–C interaction. In addition, we found here, that a higher level of Pt ions was dissolved in the electrolyte from the Pt–Pd/C electrocatalyst than from the Pt–Co/C one (Fig. 5a). To explain why, it is necessary to take into account the composition of the Pt-based alloy and also the standard reduction potential of the metal ions. As demonstrated in Table 1, the Pt content in the Pt–Co/C electrocatalyst was 1.66-fold greater than that in the Pt–Pd/C electrocatalyst. The rate of Pt re-deposition on the carbon substrate having a high Pt content should be greater than that on a composition substrate with a low Pt content. In addition, the standard potential of Pt ions is greater than that of Co ions, resulting in the fast re-deposition of Pt ions. In the case of the Pt–Pd/C electrocatalyst, the Pt ions have a lower standard reduction potential, resulting in a slow re-deposition rate for Pt ions compared to that for the Pd ions.

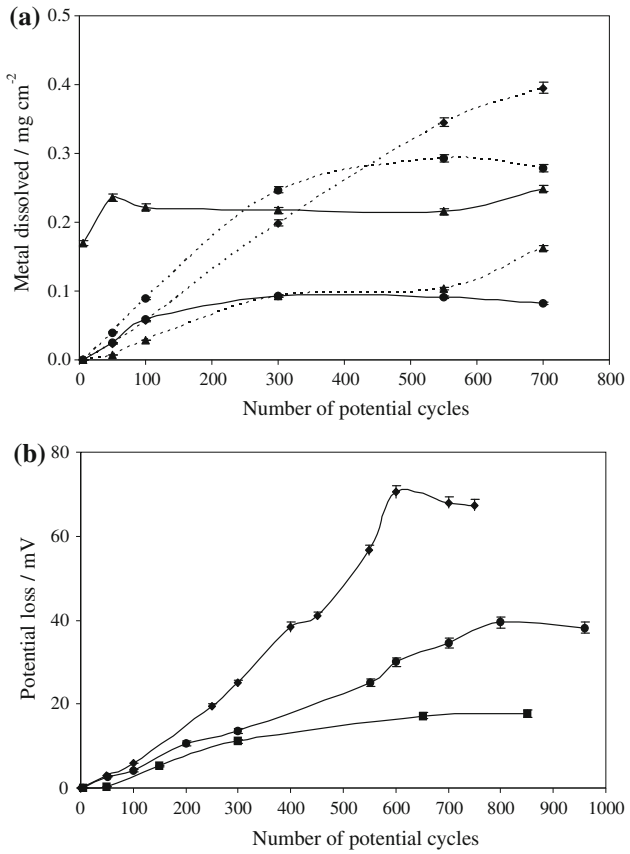

Fig. 6 **a** The dissolution of Pt (*dotted line*) and Co or Pd (*solid line*), as determined by the level of their ions in solution; and **b** the potential loss from the commercial Pt/C (*filled diamond*) and the as-prepared Pt–Co/C (*filled square*) and Pt–Pd/C (*filled circle*) electrocatalysts at a metal loading of 0.15 mg cm^{-2} after the indicated number of sequential potential cycles in 0.3 M H_2SO_4 at a scan rate of 20 mV s^{-1}

The loss of the potential due to the variation in the ESA value can be estimated by a modified Bulter–Volmer equation [45, 48, 49], as shown in Eq. 5:

$$\Delta V = b\log\left(\frac{\mathrm{ESA}_i}{\mathrm{ESA}_n}\right) \tag{5}$$

where ΔV is the cell potential drop due to the loss of Pt ESA, b is the Tafel slope at 60 °C and 1 atm (66 mV), and ESA_i and ESA_n are the initial ESA and that after potential cycling for n cycles, respectively.

As demonstrated in Fig. 6b, the potential loss due to the loss of ESA was in the order of Pt/C > Pt–Pd/C > Pt–Co/C. The maximum potential loss for the Pt/C, Pt–Pd/C and Pt–Co/C electrocatalysts was observed at 75, 39.5, and 17.3 mV after 600, 800, and 650 repeat potential cycles, respectively, and they remained essentially constant afterwards. Related to the quantity of metal ions dissolved in the electrolyte (Fig. 6a), it can be speculated that the loss of cell voltage for the Pt/C electrocatalyst might be due to the dissolution of Pt from the electrocatalyst into the electrolyte, while the loss of cell potential for the Pt–Co/C and Pt–Pd/C electrocatalysts might be due to the loss of either the Pt or the second metal (Pd or Co) from the electrocatalyst. Thus, the performance loss of Pt–Pd/C is likely to be mainly caused by Pt dissolution, while the performance loss of Pt–Co/C was mainly attributed to the dissolution of Co instead of Pt into the electrolyte.

3.3 Electrocatalyst stability test in the fuel cell environment

To further investigate the loss of cell performance in the fuel cell environment, all three types of electrocatalyst were used to prepare their respective MEA at a metal loading of 0.5 mg cm^{-2}. Their performances were then tested in a H_2/O_2 PEM fuel cell at ambient pressure and 60 °C after 5–100 repeated potential cycles.

Figure 7 displays the performance curve of the Pt–Co/C MEA after repeated potential cycling between −0.4 to +1.4 V for 5, 50, and 100 cycles at a scan rate of 50 mV s^{-1}. The performance of the fuel cell decreased with increasing numbers of repeated potential cycles, and this loss of performance was more marked the higher the number of repeated potential cycles. Thus, the loss of cell performance was likely to be due to the loss of the electrocatalyst's ESA. The deterioration in the fuel cell performance was not only observed in the activation region at high cell potentials but was also significantly seen during the ohmic region at medium- through to low- cell potentials. A similar pattern of performance degradation as a function of the number of repeated potential cycles was also observed with the Pt/C and Pt–Pd/C electrocatalysts (data not shown). Therefore, repeated potential cycling not only affected the electrocatalytic activity but also the total resistance of the fuel cell. One possible mechanism for the loss of cell performance at a high cell potential might be due to electrocatalyst dissolution [45], while that for the loss at medium to low cell potentials might be related to the corrosion of the carbon support, resulting in an increased cell resistance. Indeed, corrosion of the carbon support can subsequently induce the sintering and agglomeration of the electrocatalyst, leading to an increased size of the electrocatalyst particles and a decreased electrocatalytic activity [50].

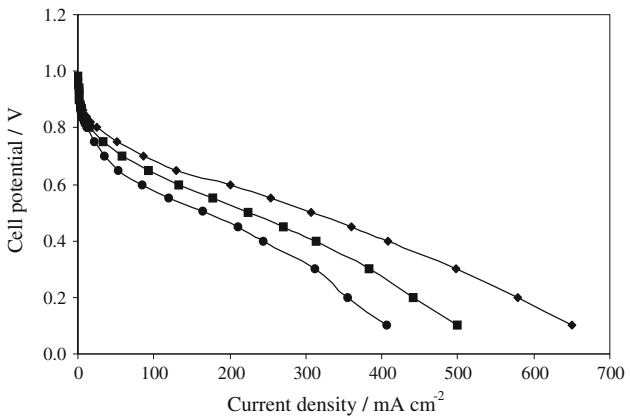

Fig. 7 Performance curve of the as-prepared Pt–Co/C electrocatalyst at a metal loading of 0.15 mg cm^{-2} after the indicated number of repeated potential cycles of 5 (*filled diamond*); 50 (*filled square*) and 100 cycles (*filled circle*) between −0.4 to +1.4 V at scan rate of 20 mV s^{-1}

The loss of the electrocatalytic activity after any particular number of repeated potential cycles was estimated from Eq. 6 [39]:

$$A_{\text{loss}}(\%) = 100 - \frac{A_n}{A_i} \times 100 \tag{6}$$

where A_i and A_n are the initial activity and the activity after n cycles, respectively, measured in terms of the current density.

The total resistance of the polarization components (R), including the charge transfer resistance for the ORR, electrolyte, and mass transfer resistance of each MEA, was calculated by the semi-empirical equation proposed by Ticianelli et al. [51] and shown in Eq. 7:

$$E = E^0 - blogi - iR \tag{7}$$

where E is the cell potential, E^0 is the standard potential, i is the current density and b is the Tafel slope. The higher the Tafel slope, the faster the overpotential increases with the current. Thus, to obtain a high current at a low overpotential, the reaction should demonstrate a low Tafel slope [52].

Table 2 exhibits the loss of electrocatalytic activity at 0.75 V, the Tafel slope and the total resistance of the commercial Pt/C and the as-prepared Pt–Co/C and Pt–Pd/C electrocatalysts after 5, 50, and 100 repeated potential cycles. The activity loss, Tafel slope and total resistance all increased as the number of repeated potential cycles increased for all three electrocatalysts. The lowest activity loss, Tafel slope and total resistance were all observed for the Pt–Co/C electrocatalyst, while the highest were all

Table 2 Loss of electrocatalytic activity (A_{loss}) at 0.75 V, the Tafel slope (b) and the total resistance (R) of the commercial Pt/C electrocatalyst and the as-prepared Pt–Pd/C and Pt–Co/C electrocatalysts with increasing numbers of repeated potential cycles

Cycle numbers	A_{loss} (%)			b (mV dec^{-1})			R (Ω-cm^2)		
	Pt/C	Pt–Co/C	Pt–Pd/C	Pt/C	Pt–Co/C	Pt–Pd/C	Pt/C	Pt–Co/C	Pt–Pd/C
5	–	–	–	73.5	65.8	71.1	4.13	0.50	0.66
50	73.5	36.7	47.0	79.8	86.0	84.6	5.32	1.11	1.13
100	75.0	59.0	62.1	107.9	101.3	100.3	9.92	1.26	1.76

obtained for the commercial Pt/C electrocatalyst, indicating the higher stability of the Pt–Co/C electrocatalyst in the fuel cell environment compared to the commercial Pt/C and as-prepared Pt–Pd/C electrocatalysts.

4 Conclusion

The stability of the Pt–Co/C and Pt–Pd/C electrocatalysts prepared at a low temperature by a combined impregnation and seeding process was evaluated by repeated potential cycling in both an acid solution and in a fuel cell environment. The loss of the catalyst ESA and the deterioration of the fuel cell performance both increased as the number of potential cycles increased, likely to be due to dissolution and re-deposition of metals from the supported Pt or Pt-M based electrocatalysts. The introduction of Co or Pd into the Pt electrocatalyst structure reduced both the loss of ESA and the deterioration of the fuel cell performance. Of the three investigated electrocatalysts, the as-prepared Pt–Co/C exhibited the highest electrocatalytic stability in both the acid electrolyte and in the fuel cell environment.

Acknowledgments The authors would like to thank the Faculty of Science, Chulalongkorn University, for financial support. The Higher Education Research Promotion and National Research University Project of Thailand, Office of the Higher Education Commission (EN276B) plus the Thai Government Stimulus Package 2 (TKK2555), under the Project for Establishment of a Comprehensive Center for Innovative Food, Health Products and Agriculture are thanked for facility support. Also, we thank the Publication Counseling Unit (PCU) of the Faculty of Science, Chulalongkorn University, and Dr. Robert D.J. Butcher for comments, suggestions and checking the grammar.

References

1. Shinichi H, Jumbom K, Supramaniam S (1997) Electrochim Acta 4(10):1587
2. Bron M, Bogdanoff P, Fiechter S, Hilgendorff M, Radnik J, Dorbandt I, Schulenburg H, Tributsh H (2001) J Electroanal Chem 517(1–2):85
3. Bezerra CWB, Zhang L, Liu H, Lee K, Marques ALB, Marques EP, Wang H, Zhang J (2007) J Power Source 173(2):891
4. Bar-On I, Kirchain R, Roth R (2002) J Power Source 109:71
5. A.D. Little, Inc. (ADL), (2011) Cost analysis of fuel cell system for transportation: baseline system cost estimate, prepared by E.J. Carlson and S. Mariano. http://www.ott.doe.gov/pdfs/baseline_cost_model.pdf. Accessed 11 Aug 2011
6. Lomax FD Jr, James BD, Baum GN, Thomas CE (1997) Detailed manufacturing cost estimates for polymer electrolyte membrane (PEM) fuel cell for light duty vehicles. Directed Technologies Inc, Arlington
7. Vante NA, Tributsch H (1986) Nature 323:431
8. Fernández JL, Raghuveer V, Manthiram A, Bard AJ (2005) J Am Chem Soc 127:13100
9. Bagotsky VS (2009) Fuel cells, problems and solution, Chap 2. Wiley, New York
10. Bashyam R, Zelenay P (2006) Nature 443:63
11. Zelenay P (2009) Advanced cathode catalysts, Hydrogen program annual merit review and peer evaluation meeting. Arlington, Virginia, May 18–22
12. Ma Y, Zhang H, Zhong H, Xu T, Jin H, Tang Y, Xu Z (2010) Electrochim Acta 55(27):7945
13. Kim SH, Pitsch H (2009) J Electrochem Soc 156(6):B673
14. Mukherjee PP, Wang CY (2007) J Electrochem Soc 154(11): B1121
15. Wang G, Mukherjee PP, Wang CY (2006) Electrochim Acta 51(15):3139
16. Wang G, Mukherjee PP, Wang CY (2006) Electrochim Acta 51(15):3151
17. Yoon YG, Yang TH, Park GG, Lee WY, Kim CS (2003) J Power Source 118(1–2):189
18. Song D, Wang Q, Zhongsheng LZ, Navessin T, Holdcroft S (2004) Electrochim Acta 50(2–3):731
19. Wang Y, Feng X (2009) J Electrochem Soc 156(3):B403
20. He T, Kreidler E, Xiong L, Luo J, Zhong CJ (2006) J Electrochem Soc 153:A1637
21. Luo J, Kariuki N, Han L, Wang L, Zhong CJ, He T (2006) Electrochim Acta 51(23):4821
22. Han KH, Moon YS, Han OH, Hwang KJ, Kim I, Kim H (2007) Electrochem Commun 9(2):317
23. Colón-Mercado HR, Popov PN (2006) J Power Source 155(2): 253
24. Zignani SC, Antolini E, Gonzalez ER (2008) J Power Source 182(1):83
25. Wu H, Wexler D, Wang G (2009) J Alloy Comp 488:195
26. Cho YH, Jeon TY, Lim JW, Cho YH, Ahnb M, Jung N, Yoo SJ, Yoon WS, Sung YE (2011) Int J Hydrogen Energy 36:4394
27. Antolini E, Salgado JRC, Giz MJ, Gonzalez ER (2005) Int J Hydrogen Energy 30(11):1213
28. Min M, Cho J, Cho K, Kim H (2000) Electrochim Acta 45:4211
29. Yang H, Vogel W, Lamy C, Alonso-Vante NC (2004) J Phys Chem B 108:11024
30. Xiong L, Manthiram A (2005) J Electrochem Soc 152:A697
31. Trongchuankij W, Poochinda K, Pruksathorn K, Hunsom M (2010) Renew Energy 35:2839
32. Thanasilp S, Hunsom M (2011) Electrochim Acta 56(3):1164
33. Thanasilp S, Hunsom M (2010) Fuel 89(12):3847
34. Lopes T, Antolini E, Gonzalez ER (2008) Int J Hydrogen Energy 33:5563
35. Xu JB, Zhao TS, Yang WW, Shen SY (2010) Int J Hydrogen Energy 35:8699
36. Vassos BH, Ewing GW (1983) Electroanalytical chemistry. Wiley, USA
37. Van Der Klink JJ (1999) Adv Catal 44:1
38. Lv H, Mu S, Cheng N, Pan M (2010) Appl Catal B 100:190
39. Huang SY, Ganesan P, Popov BN (2011) Appl Catal B 102:71
40. Colón-Mercado HR, Kim H, Popov BN (2004) Electrochem Com 6(8):795
41. Paulus UA, Wokaun A, Scherer GG, Schmidt TJ, Stamenkovic V, Markovic NM, Ross PN (2002) Electrochim Acta 47:3787
42. Yin S, Mu S, Lv H, Cheng N, Pan M, Fu Z (2010) Appl Catal B 93:233
43. Gojkovic SL, Zecevic SK, Savinell RF (1998) J Electrochem Soc 145:3712
44. Ralph TR, Hogarth MP (2002) Platin Met Rev 46:3
45. Yu P, Pemberton M, Plasse P (2005) J Power Source 144:11
46. Gasteiger HA, Kocha SS, Sompalli B, Wagner FT (2005) Appl Catal B 56:9
47. Cho YH, Choi B, Cho YH, Park HS, Sung YE (2007) Electrochem Commun 9(3):378
48. Prentice G (1991) Electrochemical engineering principles. Prentice Hall Inc., New Jersey

49. Lobato J, Cañizares P, Rodrigo MA, Linares JJ (2007) Electrochim Acta 52(12):3910
50. Huang SY, Ganesan P, Popov BN (2010) Appl Catal B 96:224
51. Ticianelli EA, Derouin CR, Redondo A, Srinivasan S (1988) J Electrochem Soc 135:2209
52. Song C, Zhang J (2008) Electrocatalytic oxygen reduction reaction. In: Zhang J (ed) PEM fuel cell electrocatalysts and catalyst layers: fundamentals and applications. Springer, London